

Magnetic order and local spin correlations in a -(Fe_{1-x}Mn_x)₇₈Sn₂Si₆B₁₄

A. Kuprin, D. Wiarda,* and D. H. Ryan

Department of Physics and Centre for the Physics of Materials, McGill University, 3600 University Street, Montreal, Quebec, Canada H3A 2T8

(Received 2 March 1999)

⁵⁷Fe and ¹¹⁹Sn Mössbauer spectroscopy has been used to study local spin correlations in site-frustrated a -(Fe_{1-x}Mn_x)₇₈Sn₂Si₆B₁₄ alloys. Comparison of total magnetization, hyperfine fields at the magnetic Fe, and nonmagnetic Sn sites shows that the Mn moments order antiparallel to the majority Fe moments and that the order established at the transverse spin freezing transition, T_{xy} , exhibits strong antiferromagnetic correlations in the plane perpendicular to the ferromagnetic axis. This result stands in strong contrast with the bond-frustrated case of a -Fe_{100-x}Zr_x, but is fully consistent with recent numerical simulations of short-ranged models. The clear difference between site- and bond-frustrated systems below T_{xy} demonstrates the importance of short-range interactions in real spin-glass systems.

INTRODUCTION

The infinite-ranged interactions implicit in mean-field spin-glass models¹ make all forms of exchange frustration equivalent. However, real systems are generally dominated by shorter-ranged interactions, and for the case of first-neighbor-only exchange coupling, two distinct situations can be identified: (i) bond frustration and (ii) site frustration.

Bond frustration arises when each exchange bond to a moment's nearest neighbors may be either positive [i.e., ferromagnetic (FM)] or negative [i.e., antiferromagnetic (AF)]. Perhaps the best experimental example of this case is provided by iron-rich a -Fe_{100-x}Zr_x^{2,3}. Here the competing exchange interactions arise from the distance dependence of the direct Fe-Fe exchange coupling [$J(r)$] combined with the distribution of nearest-neighbor distances inherent to the glass structure. With no frustration, the material is a ferromagnet, with infinite-ranged correlations and collinear order. As frustration is introduced, the order at $T=0$ becomes increasingly noncollinear and the magnetization is reduced. The ground state appears to be an xy spin glass coexisting with perpendicular ferromagnetic order (i.e., along the z axis). On heating from zero temperature, the xy spin glass melts at T_{xy} to form a collinear ferromagnet with substantial transverse degrees of freedom that fluctuate rapidly and time average to zero. Further heating takes the system to T_c where the ferromagnet undergoes a conventional three-dimensional (3D) Heisenberg phase transition to a paramagnetic state. As the degree of frustration increases, the features characteristic of ferromagnetic order decline (both T_c and magnetization fall) while spin-glass character becomes more pronounced (T_{xy} rises and irreversibilities at low temperatures become stronger). Eventually, T_c and T_{xy} meet, and further increase in frustration lead to a pure 3D spin glass (SG) with a transition temperature (T_{sg}) that is largely independent of the frustration level. The experimental observations³ are in quantitative agreement with Monte Carlo simulations of a bond-frustrated Heisenberg spin system.⁴

Site frustration is achieved by introducing a dopant with AF coupling to all of its nearest neighbors so that the frustration is introduced site wise rather than bond wise. While

the gross magnetic behavior is essentially the same as the bond-frustrated case (the system exhibits noncollinear order at low temperatures, there are two magnetic transitions at intermediate dopings and a spin glass at higher dopings), numerical simulations show that there are two striking differences.⁵ First, low levels of doping do not cause frustration. Isolated AF-coupled sites simply order antiparallel to the majority FM order, reducing the total magnetization, but not causing any noncollinearity. Frustration only appears when the dopant density is high enough for AF-AF pairs to occur. Second, the transverse correlations below T_{xy} exhibit short-range AF character rather than forming the xy spin glass observed in the bond frustrated case.

Manganese-doped systems provide the most obvious experimental examples of site-frustration, and behavior consistent with the numerical simulations is clearly seen. The amorphous (Fe,Mn)-G alloy series represent a highly studied example of site frustration. Typically they contain 75–80 at. % metals with the balance being made up from a mixture of glass-former elements (B, Al, C, Si, Sn, and P). Two magnetic transitions are observed beyond the threshold for the appearance of frustration, and these transitions merge at high Mn doping to yield a spin glass. Indeed, the strong similarities in the phase diagrams of a -(Fe_xMn_{1-x})₇₅P₁₆B₆Al₃,^{6–10} a -(Fe_xMn_{1-x})₇₅P₁₅C₁₀,¹¹ a -(Fe_xMn_{1-x})₇₇Si₁₀B₁₃,¹² and a -(Fe_{1-x}Mn_x)₇₈Sn₂Si₆B₁₄ (present work) serves to emphasize that it is the frustration introduced by the Mn that dominates the magnetic response and that the properties of the glass-former mix are largely unimportant. Crystalline Fe_{3-x}Mn_xSi yields a very similar phase diagram¹³, but also provides a direct confirmation of AF ordering perpendicular to the dominant FM order at T_{xy} .¹⁴ Polarized neutron scattering in an applied field on a single crystal of Fe₂MnSi showed that the transverse spin components that order at T_{xy} are indeed orthogonal to the FM order established at T_c and they exhibit AF correlations, in full agreement with the predictions of the numerical simulations.⁵

We present here a study of magnetization and transferred hyperfine field data for a series of a -(Fe_{1-x}Mn_x)₇₈Sn₂Si₆B₁₄ samples doped with ¹¹⁹Sn in order to determine the nature of

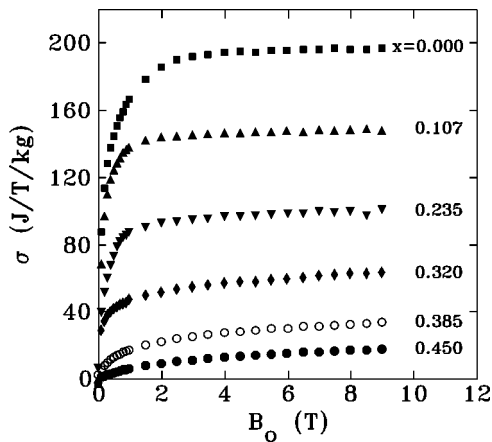


FIG. 1. Magnetization of $a\text{-(Fe}_{1-x}\text{Mn}_x\text{)}_{78}\text{Sn}_2\text{Si}_6\text{B}_{14}$ at 5 K as a function of applied magnetic induction.

the local spin correlations that develop at T_{xy} . The results show that the Mn moments order antiparallel to the FM order of the Fe moments, and that in the composition range where two transitions occur, the transverse correlations are indeed AF over the first two neighboring shells.

EXPERIMENTAL METHODS

The alloys were prepared by arc melting the appropriate ratio of pure elements (Fe: 99.95%, Mn: 99.9%, B 99.99% and Si 99.999% pure) with isotopically separated ^{119}Sn under Ti-gettered argon to yield ~ 3 g ingots. Melt spinning was carried out under a partial pressure of helium onto a copper wheel at 55 m/s. Absence of crystallinity was confirmed using $\text{Cu-K}\alpha$ powder x-ray diffraction, thermogravimetric analysis (TGA) in a small field gradient, and room-temperature Mössbauer spectroscopy.

Magnetization (shown in Fig. 1) and susceptibility data were obtained on a commercial system in fields of up to 9 T over the temperature range 5–300 K. Curie temperatures were obtained from χ_{ac} , bulk magnetization, and Mössbauer spectroscopy for those samples that ordered below 300 K, and by TGA in the cases where T_c was above 300 K.

Mössbauer measurements were made on a constant acceleration spectrometer with a 1 GBq $^{57}\text{CoRh}$ source for ^{57}Fe and a 0.1 GBq $\text{Ba}^{119\text{m}}\text{SnO}_3$ source for ^{119}Sn . All spectra were calibrated using an $\alpha\text{-Fe}$ foil. Samples were mounted in a vibration-isolated closed-cycle fridge for spectra at temperatures down to 12 K. Representative ^{57}Fe and ^{119}Sn Mössbauer spectra for the alloys studied here are shown in Figs. 2 and 3, respectively. The spectra were fitted using an asymmetric Gaussian distribution of hyperfine fields with independent widths above and below the most probable field. This was found to be the simplest, stable, form that would reproduce the observed spectra. A linear correlation between B_{hf} and the isomer shift was included to account for the slight asymmetry in the spectra. A Gaussian distribution of quadrupole splittings was used to fit those spectra obtained above T_c . All isomer shifts quoted here are relative to $\alpha\text{-Fe}$ at RT.

BASIC CHARACTERIZATION

Magnetization at 5 K (Fig. 1) shows the evolution from square, readily saturated ferromagnetic behavior to highly

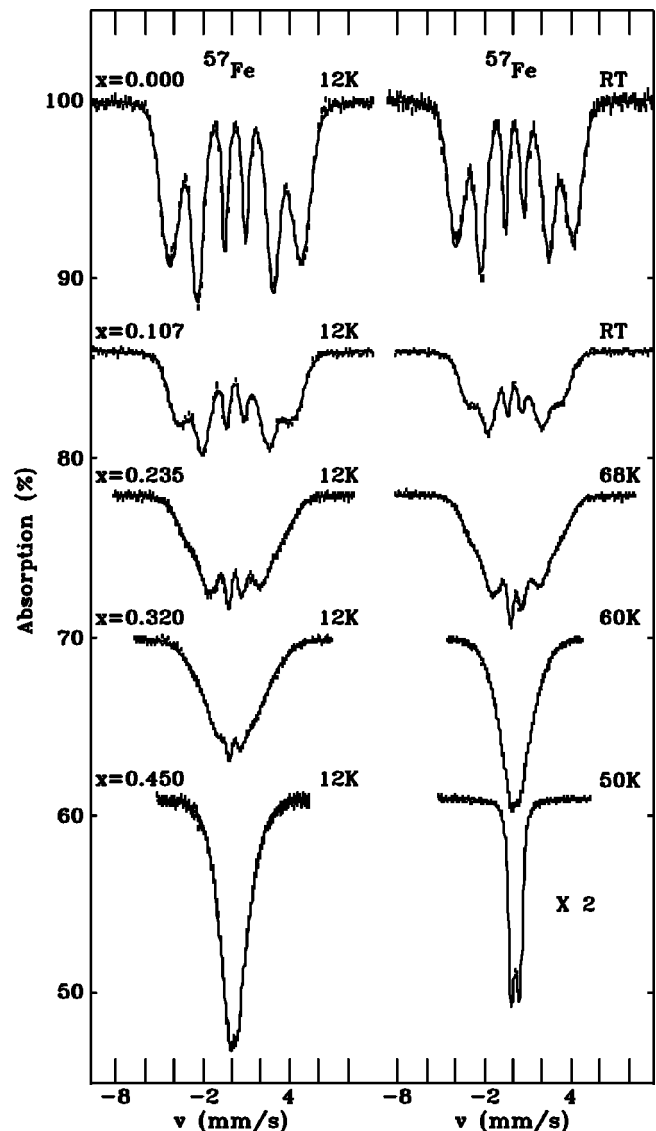


FIG. 2. ^{57}Fe Mössbauer spectra, with fits, of $a\text{-(Fe}_{1-x}\text{Mn}_x\text{)}_{78}\text{Sn}_2\text{Si}_6\text{B}_{14}$ measured at 12 K (left column) and various temperatures (right column) illustrate the magnetic state for different compositions: $x=0.000$, $x=0.107$ at RT (only a slight reduction of average hyperfine magnetic field), $x=0.235$, $x=0.320$ at 68 and 60 K, respectively (just above T_{xy}), $x=0.450$ at 50 K (complete collapse of magnetic hyperfine splitting above T_c).

curved with reduced saturation as the Mn content is increased and the system evolves from ferromagnet to spin glass. Magnetic transition temperatures (derived from both bulk magnetic, ^{57}Fe Mössbauer measurements and TGA, and shown in Fig. 4) show the expected rapid decline in T_c and the appearance of T_{xy} . The results shown in Figs. 1 and 4 are in good agreement with the results of studies on other $a\text{-(Fe,Mn)-G}$ systems.^{6,9,11,12}

The average isomer shift $\langle\delta\rangle$ reflects the total density of s electrons at the site of a probe nucleus and thus provides information about electronic configuration and chemical bonding. On warming from 12 K to RT $\langle\delta\rangle_{\text{Fe}}$ dropped from 0.24 ± 0.03 mm/s to 0.10 ± 0.04 mm/s (^{57}Fe) and $\langle\delta\rangle_{\text{Sn}}$ dropped from 1.78 ± 0.02 mm/s to 1.70 ± 0.04 mm/s (^{119}Sn). This is consistent with the contribution from the second-order Doppler shift and in accordance with data for ^{57}Fe in

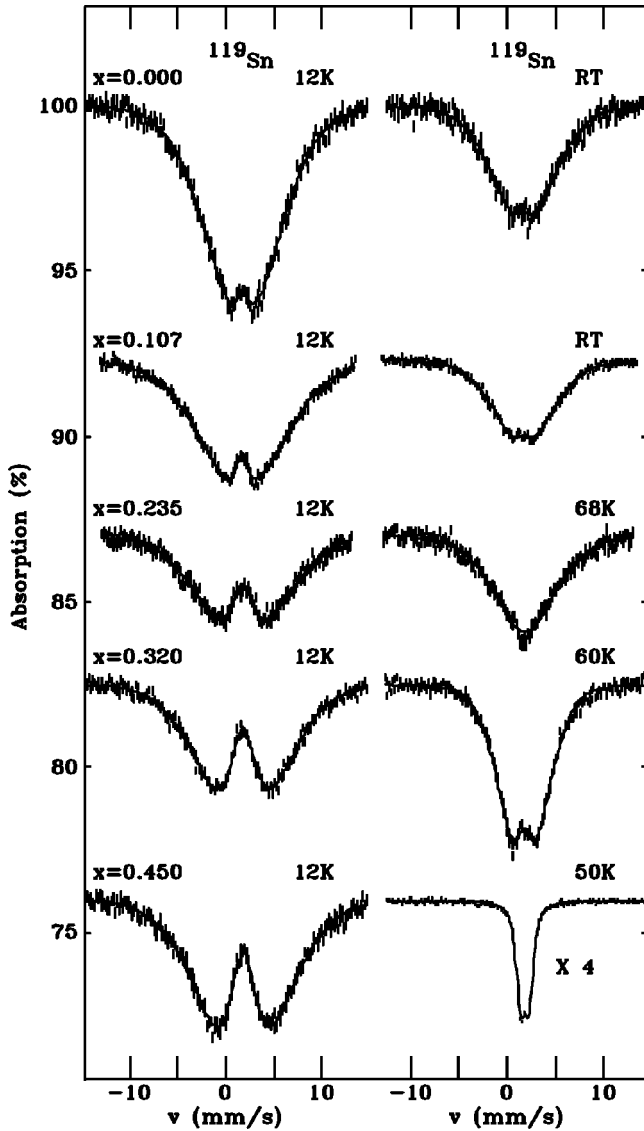


FIG. 3. ^{119}Sn Mössbauer spectra, with fits, of $a\text{-(Fe}_{1-x}\text{Mn}_x\text{)}_{78}\text{Sn}_2\text{Si}_6\text{B}_{14}$ measured at 12 K (left column) and temperatures shown in Fig. 2 (right column) illustrate the transfer of hyperfine fields from magnetic moments of surrounding Fe atoms to the nonmagnetic Sn probe.

$a\text{-(Fe}_x\text{Mn}_{1-x}\text{)}_{75}\text{P}_{15}\text{C}_{10}$ (Ref. 11) and ^{119}Sn in iron.¹⁵ $\langle\delta\rangle_{\text{Fe}}$ also dropped slightly with increasing manganese content x with a fitted slope of $0.0015(2) \text{ mm s}^{-1} (\text{at. \%})^{-1}$. This is consistent with a transfer of Fe-3d electrons to the Mn d band^{16,17} leading to a reduced shielding of 3s and 4s electrons.¹⁸ By contrast, $\langle\delta\rangle_{\text{Sn}}$ is essentially constant (data are presented in Table I), implying that the bonding of the tin atoms is not significantly affected by addition of manganese. The average quadrupole splitting $\langle\Delta\rangle$, which reflects departures from spherical symmetry in the local chemical environment, is not affected by Mn additions for either ^{57}Fe or ^{119}Sn . This observation, coupled with the weak effects on $\langle\delta\rangle$ points to the essentially unchanged electronic configuration of both tin and iron atoms with addition of manganese in the range of interest.

The average hyperfine fields ($\langle B_{\text{hf}} \rangle$) at the ^{57}Fe and ^{119}Sn sites provide complementary information on the microscopic ordering of moments in these alloys. For the purpose of the

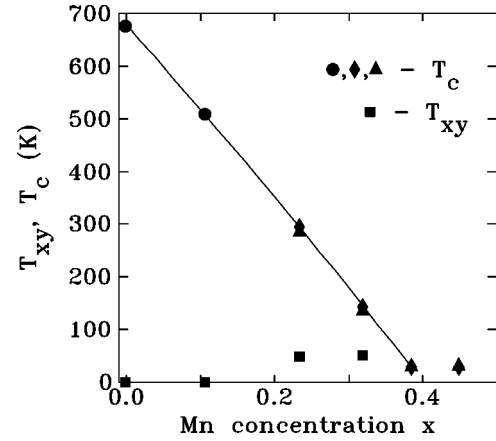


FIG. 4. Magnetic phase diagram for $a\text{-(Fe}_{1-x}\text{Mn}_x\text{)}_{78}\text{Sn}_2\text{Si}_6\text{B}_{14}$ derived from temperature dependences of the average ^{57}Fe hyperfine field (triangles and boxes) and by thermogravimetric analysis (TGA) (circles), and from measurements of bulk magnetization (diamonds).

present study it is natural to distinguish (see one of the first reviews on hyperfine interactions in iron-based alloys¹⁹) between the local contribution to the hyperfine field on ^{57}Fe which arises from the total magnetic moment μ_{loc} of the probe iron atom, and nonlocal contributions, from surrounding magnetic atoms via conduction electron polarization. For ^{119}Sn , which is nonmagnetic, the hyperfine field is transferred from moments associated with the magnetic atoms: both nearest neighbor and in more distant coordination spheres.^{20–23} Mössbauer probe atoms with zero intrinsic magnetic moment (e.g., ^{197}Au) have been used as an indicator of local correlations in the directions of moments on Fe atoms in AuFe spin-glass alloys.²⁴ The approach was extended to the use of ^{119}Sn for the same system in Ref. 25, and applied later to amorphous iron-rich metallic glasses.^{26–30}

The temperature dependence of $\langle B_{\text{hf}} \rangle$ for ^{57}Fe and ^{119}Sn ,

TABLE I. Basic characteristics derived from temperature dependences of the average hyperfine fields on ^{57}Fe and ^{119}Sn in $a\text{-(Fe}_{1-x}\text{Mn}_x\text{)}_{78}\text{Sn}_2\text{Si}_6\text{B}_{14}$ with different compositions: the Curie temperature is T_c , the temperature of transverse spin freezing is T_{xy} , the average field in the direction of bulk magnetization $\langle B_{\text{hf}}^z \rangle$ at 12 K, the total average field $\langle B_{\text{hf}}^{\text{tot}} \rangle$ at 12 K, together with the average isomer shift $\langle\delta\rangle$ at 12 K, and the average quadrupole splitting Δ at RT.

		x	0.000	0.107	0.235	0.320	0.450	\pm
^{57}Fe	T_c (K)		677	509	284	136	31	2
	T_{xy} (K)				49	52	31	2
	$\langle B_{\text{hf}}^z \rangle$ (T)		27.9	22.8	14.0	7.4		0.2
	$\langle B_{\text{hf}}^{\text{tot}} \rangle$ (T)		27.9	22.8	15.8	12.5	6.1	0.2
	$\langle\delta\rangle$ (mm/s)		0.24	0.23	0.18	0.18	0.16	0.02
	$\langle\Delta\rangle$ (mm/s)				0.58	0.60	0.57	0.02
^{119}Sn	$\langle B_{\text{hf}}^z \rangle$ (T)		5.7	6.7	5.1	4.0		0.3
	$\langle B_{\text{hf}}^{\text{tot}} \rangle$ (T)		5.7	6.7	7.3	7.5	7.7	0.3
	$\langle\delta\rangle$ (mm/s)		1.78	1.75	1.78	1.80	1.82	0.02
	$\langle\Delta\rangle$ (mm/s)				0.82	0.82	0.81	0.05

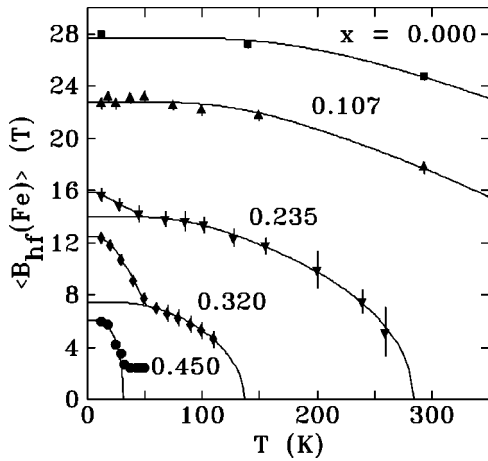


FIG. 5. Average ^{57}Fe hyperfine fields derived from Mössbauer spectra for different compositions of $a\text{-(Fe}_{1-x}\text{Mn}_x)_{78}\text{Sn}_2\text{Si}_6\text{B}_{14}$. Fits of temperature dependences are also shown. Alloys with $x=0.000$, $x=0.107$, and $x=0.450$ show a smooth temperature dependence which was fitted by a modified Brillouin function, while those with $x=0.235$ and $x=0.320$ exhibit a pronounced kink at the transverse-spin freezing temperature T_{xy} ; fits with a combined modified Brillouin function and linear term are shown below T_{xy} and with a modified Brillouin function only above T_{xy} .

shows a clear break in slope for all but the most Mn-rich and Mn-poor alloys. This behavior is expected, as it is only for intermediate Mn contents (and hence intermediate frustrations) that two magnetic transitions (T_c and T_{xy}) are predicted.⁵ The increase in $\langle B_{\text{hf}} \rangle$ with no increase in magnetization on cooling through T_{xy} is characteristic of transverse-spin freezing and reflects the ordering of spin components in the xy plane perpendicular to the FM order established parallel to, and defining, the z axis at T_c .³¹ Starting with the ^{57}Fe data, presented in Fig. 5, those alloys that exhibit no break in slope were fitted using a modified Brillouin function that includes the effects of exchange variations.³² These fits yield T_c and the average hyperfine field due to the ferromagnetic order along the z axis extrapolated to $T=0$ K: $\langle B_{\text{hf}}^z \rangle$. The break in slope was modeled by including a second modified Brillouin function to obtain fitted values for $\langle B_{\text{hf}}^{\text{tot}} \rangle$, the total hyperfine field extrapolated to $T=0$ K. However, we found that a linear increase in $\langle B_{\text{hf}} \rangle$ gave a better fit near T_{xy} , and this form was used to determine T_{xy} . The average transverse field arising from the xy components of the magnetic moments can be calculated from

$$(\langle B_{\text{hf}}^{\text{xy}} \rangle)^2 = (\langle B_{\text{hf}}^{\text{tot}} \rangle)^2 - (\langle B_{\text{hf}}^z \rangle)^2.$$

The behavior of the field at ^{119}Sn sites shows similar compositional behavior, with kinks at approximately the same temperature seen for ^{57}Fe . However, there is a strong deviation from a Brillouin-like course in the form of a much steeper decline in comparison with ^{57}Fe (Fig. 6). This is well known in crystalline magnetic alloys, where the difference between the reduced hyperfine field and the reduced magnetization of the host is called the “temperature anomaly.” This anomaly introduces an additional uncertainty into the determination of $\langle B_{\text{hf}}^z \rangle$ and hence of $\langle B_{\text{hf}}^{\text{xy}} \rangle$ for ^{119}Sn in samples that exhibit kinks in $\langle B_{\text{hf}} \rangle(T)$. In these cases the value of $\langle B_{\text{hf}}^z \rangle$ at $T=0$ K was estimated from the value at

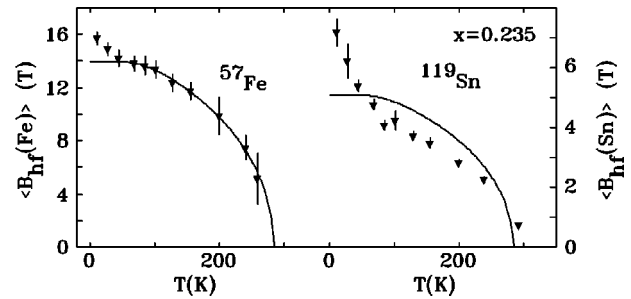


FIG. 6. Comparison of the temperature dependence of the average ^{57}Fe (left) and ^{119}Sn (right) hyperfine fields for $a\text{-(Fe}_{1-x}\text{Mn}_x)_{78}\text{Sn}_2\text{Si}_6\text{B}_{14}$ with $x=0.235$. The fit of the dependence for ^{57}Fe at temperatures above T_{xy} by a modified Brillouin function is also shown; it is scaled to the $\langle B_{\text{hf}}^z(\text{Sn}) \rangle$ value at $T=0$ K on the right. The much steeper decrease in the average ^{119}Sn hyperfine field demonstrates the strong temperature anomaly for ^{119}Sn (see details in the text).

$T=0.5 T_c$ where $B_{\text{hf}}(T) \sim 0.85 B_{\text{hf}}(0)$ according to experimental data on ^{119}Sn in iron ferromagnets^{21,22}.

The results of fits to both the ^{57}Fe and ^{119}Sn data are given in Table I. The fitted fields are plotted vs x in Fig. 7. The phase diagram for this system (Fig. 4) is consistent with those of similar amorphous FeMn-G systems [e.g., $a\text{-(Fe}_x\text{Mn}_{1-x})_{75}\text{P}_{16}\text{B}_6\text{Al}_3$ (Ref. 10) and

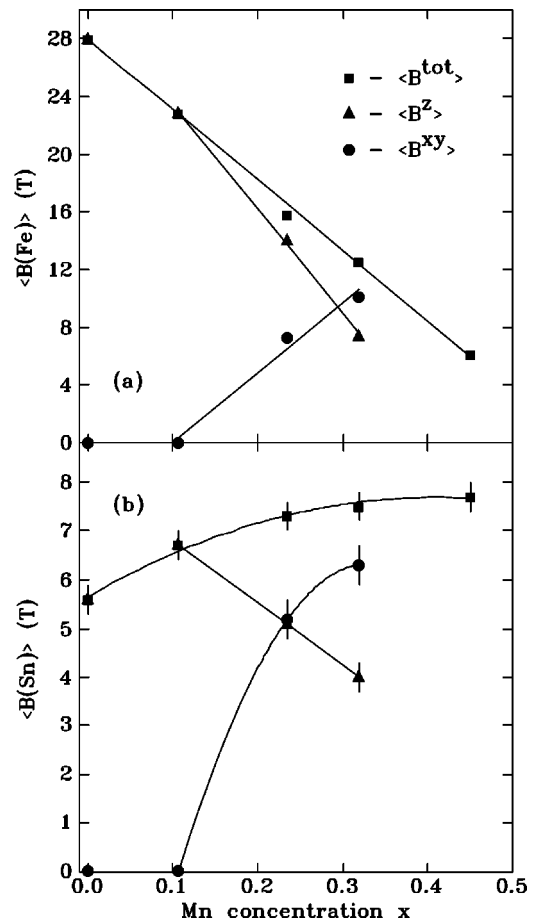


FIG. 7. Concentration dependence of the average $|\langle B_{\text{hf}}^{\text{tot}} \rangle|$, $|\langle B_{\text{hf}}^z \rangle|$, and $|\langle B_{\text{hf}}^{\text{xy}} \rangle|$ extrapolated to zero temperature for ^{57}Fe (a) and ^{119}Sn (b). Solid lines are guides to the eye.

a -(Fe_xMn_{1-x})₇₇Si₁₀B₁₃ (Ref. 12)]. For $x=0$ and $x=0.107$ the samples are ferromagnetic for all temperatures below T_c , while for $x=0.235$ and $x=0.320$ two magnetic transitions are evident. Finally, for $x \geq 0.385$, the system is a spin glass.

The primary purpose of the present study is to use the temperature and composition dependences of the ^{57}Fe and ^{119}Sn hyperfine fields to determine the nature of the ordering that occurs at T_{xy} . The simplest model involves assuming that both fields are dominated by short-range contributions. In such a model, the ^{57}Fe field is assumed to be proportional to the local iron moment only, while in the case of ^{119}Sn the field is attributed to a vector average over the moments in the first coordination shell (the absence of a local moment on the Sn is explicitly assumed here).²⁸ This model has been applied to measurements of magnetic and nonmagnetic Mössbauer probes in several bond frustrated systems: ^{119}Sn and ^{197}Au in crystalline AuFe₁₀Sn₂ (Refs. 24 and 25) and ^{119}Sn in amorphous Fe₉₂Zr₇Sn₁ (Ref. 26) and Fe_{90-x}Ni_xZr₇Sn₁ with $x=1$ and $x=3$.³⁰ In all cases the ratio:

$$\mathcal{R}(T) = \langle B_{hf}^{\text{non-mag}} \rangle / \langle B_{hf}^{\text{Fe}} \rangle$$

was found to be constant, or only weakly temperature dependent ($< 10^{-3} \text{ K}^{-1}$). Furthermore, even in the AuFe alloys where a clear break in the temperature dependence of $\langle B_{hf} \rangle$ was observed for both the magnetic and non magnetic probes at T_{xy} ,^{24,25} no break in the slope of $\mathcal{R}(T)$ was present.²⁶ The observed proportionality between intrinsic field on ^{57}Fe and the transferred field on the nonmagnetic probe, leads, within this simple model, to the conclusion that the transverse components are aligned FM over first-neighbor distances. A result that is inconsistent with the absence of an increase in magnetization below T_{xy} , and is in direct conflict with both mean-field calculations¹ and numerical simulations⁴ which predict SG ordering of transverse components. However, the clearest indication that this simple model is inadequate comes from ^{119}Sn -doped a -Fe₉₀Sc₁₀.²⁹ This material is a spin glass with no net magnetization,^{27,33} so a zero, or at least very small, transferred field is expected at ^{119}Sn and $\mathcal{R}(T)$ should also be close to zero. However, $\mathcal{R}(T)$ was found to be the same as it is in a -Fe and the simple model clearly needs to be improved.

$\mathcal{R}(T)$ for the alloys studied here is shown in Fig. 8. Two features are immediately apparent: (i) there is a systematic increase in the ratio with increasing Mn content, which extends even to the $x=0.450$ case that is a spin glass. This increase in $\mathcal{R}(T)$ with x both above and below T_{xy} occurs even as the average magnetization clearly falls (see Fig. 1), and the ^{57}Fe field drops by a factor of 4.5 (see Fig. 5). These results serve to underline the inadequacy of the simple model outlined above. (ii) There is a clear break in the slope of $\mathcal{R}(T)$ for $x=0.235$ and $x=0.320$, the two alloys which exhibit transverse spin freezing. No such break has been observed in previous studies of bond frustrated alloys and this is strong evidence that the detailed nature of the ordering at T_{xy} in these site-frustrated materials differs from the bond-frustrated case.

ANALYSIS OF TRANSFERRED HYPERFINE FIELDS

For the purpose of the present study of the hyperfine fields at the Mössbauer probe sites we will use the approach of a

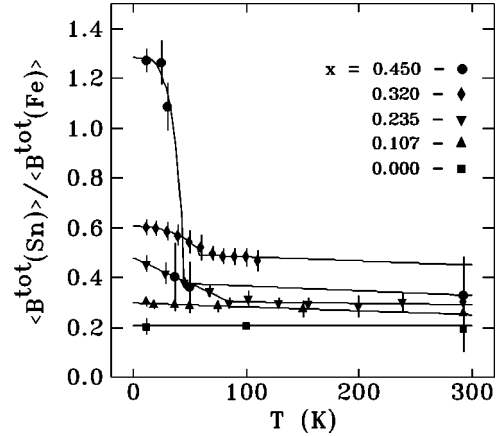


FIG. 8. Ratio of the total average transferred hyperfine field at ^{119}Sn sites to that at the ^{57}Fe sites as a function of temperature for different compositions of a -(Fe_{1-x}Mn_x)₇₈Sn₂Si₆B₁₄. Solid lines are guides to the eye.

magnetic polarization model (see detailed analysis in Ref. 34) which distinguishes between contributions local to the magnetic moment of Mössbauer probe atom and those transferred from magnetic moments on neighboring atoms. Both types of contribution act through the polarization of s -like electrons via exchange interactions with unpaired $3d$ electrons. The net polarization at the probe nucleus then induces a hyperfine field through the Fermi contact interaction.

Within this model, the average field at the nucleus of a magnetic probe atom (^{57}Fe) in an amorphous magnetic alloy in which different magnetic species are uniformly distributed over coordination spheres, may be written as a sum of two components. The first is associated with the local magnetic moment of the probe, while the second reflects the contribution from surrounding magnetic atoms:

$$\langle B_{hf}(\text{Fe}) \rangle = A \langle \mu_{\text{loc}} \rangle + B \langle \mu_1 \rangle, \quad (1)$$

where A and B are constants, $\langle \mu_{\text{loc}} \rangle$ is the magnetic moment of the probe atom (which may be affected by the species present on neighboring sites³⁴) and μ_1^{tot} is the average moment of surrounding atoms, with the main contribution to it coming from the first-nearest neighbors (1st NN).³⁴ Unfortunately, consistent values for A and B are not directly available from the literature. The theoretical problem is challenging, and as yet unsolved. Comparisons are further complicated because the decomposition terms used (core, valence, conduction electron polarization, etc.) do not map uniquely onto Eq. (1). Also most work is on collinear magnetic systems, where the only real constraint is provided by the sum $A+B$, and separating the two contributions is complex. Theoretical estimates for A range from $10 \text{ T}/\mu_B$ for Fe-V sandwiches,³⁵ $7\text{--}10 \text{ T}/\mu_B$ for FeCr and FeCo alloys³⁶ to $3.7 \text{ T}/\mu_B$ for impurities in nickel.³⁷ Experimental values include the widely used $15 \text{ T}/\mu_B$ (all local, no transferred field), $7.5 \text{ T}/\mu_B$ in (Fe,Mn)₃Al,³⁸ $4 \text{ T}/\mu_B$ at ^{55}Mn in the same alloy,³⁹ to zero, due to a cancellation of two local terms, derived for Fe-Al alloys.⁴⁰

Since there is no consensus, we adopt the following procedure to determine A and B . The first term is entirely local and the prefactor A should not be affected by chemical or magnetic environments. Its value can be estimated from ex-

TABLE II. The average magnetic moments (in μ_B) used in and derived from the present analysis. The σ is the moment of the alloy per magnetic atom. $\langle\mu_{\text{Fe}}^{\text{tot}}\rangle$ was obtained from the bulk value at $x=0.000$, and all other moments were derived from the Mössbauer data (detailed description is given in the text). The superscript z denotes longitudinal components (in the direction of domain magnetization σ , or μ_{Fe}^z) while xy denotes transverse components and tot is the total moment. The subscript 1 denotes average moment per atom of the first near-neighbour (NN) shell. The transverse components of the average moment on the 1st NN shell for the noncollinear alloys exhibiting spin-freezing transition (i.e., those with $x=0.235$ and $x=0.320$), and of the total average moment of the 1st NN shell for the complete spin glass ($x=0.450$), were also calculated assuming random orientation of transverse components $\langle\mu_{\text{Fe}}^{xy}\rangle$ and $\langle\mu_{\text{Mn}}^{xy}\rangle$ or total moments $\langle\mu_{\text{Fe}}^{\text{tot}}\rangle$ and $\langle\mu_{\text{Mn}}^{\text{tot}}\rangle$, respectively. These values are shown at the bottom of the table. A negative sign means AF alignment with respect to the direction of the corresponding component of the Fe moment.

x	0.000	0.107	0.235	0.320	0.450
σ^a	2.19 ± 0.01	1.69 ± 0.01	1.07 ± 0.01	0.59 ± 0.01	0.00
$\langle\mu_{\text{Fe}}^z\rangle$	2.19 ± 0.01	2.16 ± 0.01	1.84 ± 0.06	1.47 ± 0.07	
$\langle\mu_{\text{Fe}}^{xy}\rangle$	0.00	0.00	1.04 ± 0.11	1.48 ± 0.06	
$\langle\mu_{\text{Fe}}^{\text{tot}}\rangle$	2.19 ± 0.01	2.16 ± 0.01	2.12 ± 0.01	2.09 ± 0.01	2.04 ± 0.01
$\langle\mu_{\text{Mn}}^z\rangle$		-3.47 ± 0.50 -2.89 ± 0.10^a	-3.57 ± 0.35	-3.43 ± 0.25	
$\langle\mu_{\text{Mn}}^{xy}\rangle$		0.00	-2.39 ± 0.37	-2.25 ± 0.15	
$\langle\mu_{\text{Mn}}^{\text{tot}}\rangle$		3.47 ± 0.50 2.89 ± 0.10^a	4.29 ± 0.57	4.10 ± 0.29	3.28 ± 0.47
$\langle\mu_1^z\rangle$	2.19 ± 0.01	1.56 ± 0.05	0.57 ± 0.07	-0.10 ± 0.07	
$\langle\mu_1^{xy}\rangle$	0.00	0.00	0.24 ± 0.02	0.29 ± 0.02	
$\langle\mu_1^{\text{tot}}\rangle$	2.19 ± 0.01	1.56 ± 0.05	0.62 ± 0.06	0.31 ± 0.03	0.35 ± 0.01
$\langle\mu_{1\text{random}}^{xy}\rangle$		—	0.45 ± 0.06	0.52 ± 0.03	
$\langle\mu_{1\text{random}}^{\text{tot}}\rangle$					0.80 ± 0.08

^aObtained from measurements of bulk magnetization at 5 K extrapolated to zero field.

perimental data on the hyperfine field at the Cu nucleus in dilute FeCu alloys. Since there is no local moment on the Cu, the observed hyperfine field of -21.3 to -21.8 T (Refs. 41–43) represents the effects of nonlocal transferred hyperfine fields. Dividing by the Fe moment of $2.2\mu_B$ gives $B = -9.9$ T/ μ_B . Substituting this value for B and the -34.0 T hyperfine field observed for Fe in bulk iron at 4.2 K into Eq. (1) yields $A = 5.5$ T/ μ_B . It is important to note that the model used here differs significantly from that used previously,^{26,28} as over 60% of the observed ⁵⁷Fe field now derives from the influence of the first neighbors. The second term in Eq. (1) involves transferred fields and is, in principle, affected by the density of conduction electrons, and hence, the value of $B = -9.9$ T/ μ_B derived from bulk Fe may not always apply. Indeed, when this two-component model was applied to a variety of ferromagnetic iron-based alloys a value of $B = -8.0$ T/ μ_B (Ref. 44) was reported. Using the fact that in the $x=0$ alloy, the iron moment is equal to the value of bulk magnetization per magnetic atom (data on measured and calculated moments are summarized in Table II) and that for this case $\mu_1 = \mu_{\text{Fe}}$ we obtain $B = -7.22 \pm 0.18$ T/ μ_B which is slightly smaller than reported in other alloys.⁴⁴

Since the ¹¹⁹Sn probe has no local moment, the $\langle\mu_{\text{loc}}\rangle$ term for ¹¹⁹Sn must be zero, and any observed hyperfine field must be due entirely to the influence of neighboring moments. Any hyperfine field must arise from a polarization of occupied inner electron shells, and it has been shown ex-

perimentally that the hyperfine field on ¹¹⁹Sn can be represented as a sum of two contributions of opposite sign.^{20–23} The positive term originates from a direct interaction between polarized conduction band electrons and electrons of the filled Sn shells, while the negative term comes from an indirect polarization of the internal shells by polarized outer shell electrons.²⁰ The two terms are large and close in absolute magnitude and are in turn made up of sums of partial contributions from different coordination spheres. The negative, indirect term, is much more local in nature and the positive, direct term, prevails by the second sphere.^{21–23} This combination leads to oscillations in the radial dependence of the partial contribution to the total hyperfine field and makes the net field very sensitive to the distribution of magnetic moments over the coordination spheres. It is this sensitivity that we exploit here to determine the nature of the order below T_{xy} . The radial dependence of the partial contributions to the total hyperfine field at ¹¹⁹Sn has been determined experimentally (Ref. 45 and references therein) by analyzing data from bcc, fcc, and hcp metallic ferromagnets with different distributions of magnetic moments over the coordination spheres. Analysis of such data with the explicit assumption that the net contribution to the field from moments in spheres with radius larger than 4 \AA can be represented by a single term proportional to the average magnetization of the alloy (σ) shows that the resultant transferred hyperfine field is negative for $r < 2.8 \text{ \AA}$, has a sign reversal at $r \sim 2.9 - 3.2 \text{ \AA}$, reaches a positive maximum for $r \sim 3.5 \text{ \AA}$, and

crosses the axis again around 3.8 Å. The corresponding dependence for ^{57}Fe atoms in bcc alloys is quite similar, except that the negative contribution from nearest neighbors always dominates.

If we approximate the rather complex form described above by using two terms, the first (negative) term being due to moments in the first coordination shell, and the second (positive) term coming from all moments in more distant coordination shells, then we obtain a two-component model similar to that used for ^{57}Fe above, except that the first term of Eq. (1) is explicitly zero (no ^{119}Sn moment) and the second term is now broken up into the first coordination sphere and beyond. This two-component model has previously been used to explain the large temperature anomalies in the hyperfine field (due to a strong radial dependence of the negative contribution to the field), the correlation between temperature anomalies and thermal expansion of the lattice, and the strong pressure dependence of the field in metallic ferromagnets (Ref. 46 and references therein). Self-consistent calculations of the electronic structure of sp impurity atoms in ferromagnetic iron show a similar separation between the negative contribution to the field arising from bonding states and the positive one due to antibonding states, and also that the contribution from core polarization is small.⁴⁷

This two-component model leads to the following expression for the average field at the ^{119}Sn nucleus in our amorphous alloys:

$$\langle B_{\text{hf}}(\text{Sn}) \rangle = -C\langle \mu_1 \rangle + D\sigma, \quad (2)$$

where C and D are constants.⁴⁸ In order to proceed, we need the sign of the hyperfine field at the ^{119}Sn sites, a parameter that cannot be determined uniquely without applying an external field. However, it is reasonable to assume that for $x=0$ it is negative as it is in $\alpha\text{-Fe}$ where $B_{\text{hf}}(\text{Sn}) = -8.3 \text{ T}$.^{21,15} Furthermore, an inspection of Figs. 1, 7(a), and 7(b) shows that the ^{119}Sn field grows as the average alloy magnetization falls, suggesting that the negative term ($C\langle \mu_1 \rangle$) always dominates. Finally, the negative sign of the temperature anomaly apparent in Fig. 6 for $x=0.235$ requires that the field also be negative for this alloy.⁴⁶ Assuming therefore that the ^{119}Sn field is negative, and taking $D=20 \text{ T}/\mu_B$ from (Ref. 45), we derive $C=22.6 \pm 0.2 \text{ T}/\mu_B$ for the $x=0$ alloy. Taking the number of nearest-metal neighbors in our alloy to be close to 10 with separation $r \sim 2.57 \text{ Å}$ (estimated from experimental data on $a\text{-Fe}_{1-x}\text{B}_x$ system⁴⁹), we obtain the value of partial contribution equal to $2.3 \pm 0.2 \text{ T}/\mu_B/\text{neighbor}$, which is in rather good agreement with the value of $2.1 \pm 0.1 \text{ T}/\mu_B/\text{neighbor}$ for $r=2.59 \text{ Å}$ derived from data on Sn-doped FeRh and Fe_3Ge .⁴⁵

The volume expansion caused by introducing Mn,⁵⁰ coupled with the significant radial dependence of the contribution from the first-neighbor shell [about $14 \text{ T } \mu_B^{-1} \text{ Å}^{-1}$] (Ref. 46)] means that B and C , in Eqs. (1) and (2), respectively, must be composition dependent. A further correction should be introduced to account for a linear decrease in the total moment on Fe in accordance with the change of measured and calculated $\langle \delta \rangle$ (Ref. 51) [upper estimate of which is $\sim 10\%$ when half of Fe atoms are replaced by Mn (Ref. 11)]. This decrease in $\langle \mu_{\text{Fe}} \rangle$ also diminishes the contribution to A from s - d mixing, but the change is expected to be much

less than 10% and will not be considered here. We emphasize that while these corrections are expected from the origins of the various components and serve to improve the overall consistency of the fits, they do not in any way affect the final conclusions.

DEDUCED MAGNETIC STRUCTURES

Figure 1 shows that there is a very large reduction in the magnetization on going from $x=0$ to $x=0.107$. If we assume that the magnetic structure remains collinear, then we deduce an average Mn moment $\langle \mu_{\text{Mn}}^z \rangle = -2.89(10) \mu_B$ indicating an antiparallel ordering of the Fe and Mn moments. This is fully consistent with the absence of a second magnetic transition and with model calculations for this composition,⁵ where the Mn atoms are expected to be surrounded by Fe atoms and Mn-Mn contacts will be absent. We can also estimate the Mn moment from the ^{57}Fe hyperfine field. Equation (1) (written now for z components) gives $\langle \mu_1^z \rangle = 1.56(5) \mu_B$ and assuming additivity in the polarization of conduction electrons by Fe and Mn moments, the longitudinal component of Mn moment can be calculated from the following equation:

$$\langle \mu_{\text{Mn}}^z \rangle = [(1-x)\langle \mu_{\text{Fe}}^z \rangle - \langle \mu_1^z \rangle]/x, \quad (3)$$

where a positive value for $\langle \mu_{\text{Mn}}^z \rangle$ corresponds to AF Fe-Mn alignment. The deduced value of $\langle \mu_{\text{Mn}}^z \rangle = 3.47 \pm 0.50 \mu_B$ is somewhat larger than, but consistent with the magnetization result. This consistency provides an additional check on our selection of values for A and B in Eq. (1).

Using $\langle \mu_1^z \rangle = 1.56(5) \mu_B$ in Eq. (2) (also written for z components) and assuming collinear order, gives $D = 16.7 \pm 0.9 \text{ T}/\mu_B$, which is about 16% smaller than the value for the alloy without Mn. This decrease reflects the assumption that the net contribution to the field from magnetic moments located at distances larger than 4 Å (i.e., from all shells following the 1st NN shell) can be written as a single term proportional to σ . However, the majority of this term comes from the 2nd NN shell, and the z component of its average moment will be closer to $\langle \mu_1^z \rangle$ than to σ , the former being about 8% smaller (data are summarized in Table II). Thus the apparent drop in D stems from a limitation of the model, however, a complete accounting for further shells would introduce unwarranted complications.

The alloys with higher Mn contents are expected to have noncollinear magnetic structures⁵ and both the $x=0.235$ and $x=0.320$ samples exhibit the two magnetic transitions characteristic of partially frustrated systems (see Figs. 4 and 5). Equations (1) and (2) will be true for the z components of the fields and moments, but when applied to $\langle B_{\text{hf}}^{\text{tot}}(\text{Fe}) \rangle$ and $\langle B_{\text{hf}}^{\text{tot}}(\text{Sn}) \rangle$, respectively they should be regarded as vector equations, i.e., they should involve a dependence on the angle (α) between vectors $\langle \mu_{\text{Fe}}^{\text{tot}} \rangle$ and $\langle \mu_1^{\text{tot}} \rangle$, and the angle (θ) between vector $\langle \mu_1^{\text{tot}} \rangle$ and the z direction defined by the domain magnetization. Thus,

$$[\langle B_{\text{hf}}^{\text{tot}}(\text{Fe}) \rangle]^2 = (A\langle \mu_{\text{Fe}}^{\text{tot}} \rangle)^2 + (B\langle \mu_1^{\text{tot}} \rangle)^2 + 2AB\langle \mu_{\text{Fe}}^{\text{tot}} \rangle \times \langle \mu_1^{\text{tot}} \rangle \cos \alpha \quad (4)$$

and

$$[\langle B_{\text{hf}}^{\text{tot}}(\text{Sn}) \rangle]^2 = (C\langle \mu_1^{\text{tot}} \rangle)^2 + (D\sigma)^2 - 2CD\langle \mu_1^{\text{tot}} \rangle \sigma \cos \theta. \quad (5)$$

To proceed further, we need to assume a form for the correlations between the transverse-spin components. Two simple possibilities exist: collinear and random. The former can be further broken down into ferromagnetic and antiferromagnetic. FM alignment of transverse components would lead to a net increase in magnetization and can, in principle, be eliminated from consideration immediately. However, in what follows, we will retain this case in the interests of completeness. We deal first with the case of collinear ordering of the transverse components and then the random, or spin-glass case.

If we assume collinear alignment of the transverse components of the Fe and Mn moments, then the angles α and θ in Eqs. (4) and (5) are linked via (φ_{Fe}) the angle between the average Fe moment $\langle \mu_{\text{Fe}}^{\text{tot}} \rangle$ and the z direction:

$$\alpha = |\theta \pm \varphi_{\text{Fe}}|. \quad (6)$$

In the present model, the transverse field on ^{119}Sn arises only from the transverse component of the moments in the 1st NN shell, and the net transverse component of the 2nd and following NN shells as well as that of bulk magnetization is assumed to average to zero. In this case, Eq. (2) reduces to

$$\langle B_{\text{hf}}^{\text{xy}}(\text{Sn}) \rangle = C\langle \mu_1^{\text{xy}} \rangle, \quad (7)$$

and $\langle \mu_1^{\text{xy}} \rangle$ can be determined directly from the data. The transverse field on ^{57}Fe will depend on the transverse components of both the local Fe moment and that of the 1st NN shell. Allowing for either FM or AF alignment through the \pm sign in Eq. (6), Eq. (2) becomes

$$\langle B_{\text{hf}}^{\text{xy}}(\text{Fe}) \rangle = A\langle \mu_{\text{Fe}}^{\text{xy}} \rangle \mp B\langle \mu_1^{\text{xy}} \rangle \quad (8)$$

and allows us to find $\langle \mu_{\text{Fe}}^{\text{xy}} \rangle$ using $\langle \mu_1^{\text{xy}} \rangle$ obtained from Eq. (7). We note that there is no defined direction within the xy plane and we need only to know the respective orientation of transverse components of the moments on Fe and Mn, and hence their absolute values, which, in the approximation of the present model, are connected by an equation analogous to Eq. (3):

$$\langle \mu_{\text{Mn}}^{\text{xy}} \rangle = [(1-x)|\langle \mu_{\text{Fe}}^{\text{xy}} \rangle| \pm |\langle \mu_1^{\text{xy}} \rangle|]/x, \quad (9)$$

where again a positive value for $\langle \mu_{\text{Mn}}^{\text{xy}} \rangle$ corresponds to AF alignment with respect to $\langle \mu_{\text{Fe}}^{\text{xy}} \rangle$.

The two roots of Eq. (8) mean that two possible configurations of the moments on Fe and Mn can exist with the same values of $\langle \mu_1^{\text{xy}} \rangle$, and $\langle \mu_{\text{Fe}}^{\text{tot}} \rangle$. Configurations with AF alignment of $\langle \mu_{\text{Fe}}^{\text{xy}} \rangle$ and $\langle \mu_1^{\text{xy}} \rangle$ result in unrealistically large average total moments on Mn of about $6.3 \pm 0.4 \mu_B$ and thus will not be considered in the following discussion.

Knowing the values of $\langle \mu_{\text{Fe}}^{\text{xy}} \rangle$ and $\langle \mu_{\text{Fe}}^{\text{tot}} \rangle$ we can determine $\langle \mu_{\text{Fe}}^z \rangle$. Then, using Eq. (1) written for z components (we assume that $\langle \mu_{\text{Fe}}^z \rangle$ points in the positive z direction) one can find the value and orientation of the longitudinal component of the 1st NN shell moment:

$$\langle \mu_1^z \rangle = [\langle B_{\text{hf}}^z(\text{Fe}) \rangle - A\langle \mu_{\text{Fe}}^z \rangle]/B, \quad (10)$$

where a negative value for $\langle \mu_1^z \rangle$ corresponds to AF alignment with respect to $\langle \mu_{\text{Fe}}^z \rangle$. Finally, knowing $\langle \mu_1^z \rangle$, we can calculate the average value of the total moment of the first near-neighbors shell $\langle \mu_1^{\text{tot}} \rangle$.

For the alloy with $x=0.450$ it is impossible to separate the longitudinal and transverse components of the moments, but the fact that the spontaneous bulk magnetization σ is zero [see Fig. 1 and (Refs. 11 and 52)] allows us to derive $\langle \mu_1^{\text{tot}} \rangle$ directly from Eq. (5). Its use in Eq. (4) then gives the value of $\cos \alpha$ which can then be used to calculate the average moment on the Mn atoms using an equation analogous to Eqs. (3) and (9) which links average moments $\langle \mu_{\text{Fe}}^{\text{tot}} \rangle$, $\langle \mu_{\text{Mn}}^{\text{tot}} \rangle$, and $\langle \mu_1^{\text{tot}} \rangle$ and which now becomes a vector equation. We note that direct determination of the proportionality factor D is not possible for the complete spin-glass state, however, apart from this, we are able to determine all of the parameters for the present model. The results of this analysis are summarized in Table II.

If we repeat the analysis while assuming a random orientation of $\langle \mu_{\text{Mn}}^{\text{xy}} \rangle$ and $\langle \mu_{\text{Fe}}^{\text{xy}} \rangle$ for the alloys with $x=0.235$ and $x=0.320$, and random orientation of $\langle \mu_{\text{Fe}}^{\text{tot}} \rangle$ and $\langle \mu_{\text{Mn}}^{\text{tot}} \rangle$ for the complete spin glass with $x=0.450$ we obtain values of $\langle \mu_1^{\text{xy}} \rangle$ and $\langle \mu_1^{\text{tot}} \rangle$ that are approximately twice as large as those obtained under the assumption of AF alignment. Furthermore, the assumption of random orientation of $\langle \mu_{\text{Fe}}^{\text{xy}} \rangle$ and $\langle \mu_1^{\text{xy}} \rangle$ in Eq. (8) yields very large values for $\langle \mu_{\text{Fe}}^{\text{xy}} \rangle$ ($1.31 \pm 0.04 \mu_B$ and $1.81 \pm 0.04 \mu_B$ for $x=0.235$ and $x=0.320$, respectively). The latter value is almost the same as $\langle \mu_{\text{Fe}}^{\text{tot}} \rangle = 2.09 \pm 0.01 \mu_B$. Statistical averaging of $\langle \mu_{\text{Fe}}^{\text{xy}} \rangle$ and $\langle \mu_1^{\text{xy}} \rangle$ with weights from Eq. (9) then leads to very large values for $\langle \mu_{\text{Mn}}^{\text{xy}} \rangle$ of $4.35 \pm 0.05 \mu_B$ and $3.92 \pm 0.05 \mu_B$ for $x=0.235$ and $x=0.320$, respectively. These in turn result in unrealistically large values for $\langle \mu_{\text{Mn}}^{\text{tot}} \rangle$ of $5.63 \pm 0.35 \mu_B$ and $5.20 \pm 0.25 \mu_B$. Thus we can immediately rule out the possibility of random orientations of either the transverse components or the total moments on Fe and Mn.

Introducing φ_{Mn} the angle between the average Mn moment and the $-z$ direction (cf. φ_{Fe} defined above), we find that average total Fe and Mn moments deflect, respectively, from the $+z$ and $-z$ directions in the opposite half-planes. At $x=0.235$ their canting angles are close: $\varphi_{\text{Fe}} = 29 \pm 4^\circ$ and $\varphi_{\text{Mn}} = 34 \pm 5^\circ$ and weak frustration causes a rather small net canting of $\langle \mu_1^{\text{tot}} \rangle$ ($\theta = 22 \pm 3^\circ$). At higher frustration ($x=0.320$) the canting of the Fe moment increases ($\varphi_{\text{Fe}} = 45 \pm 5^\circ$), but remains the same for Mn ($\varphi_{\text{Mn}} = 33 \pm 3^\circ$). Nevertheless the frustration is now strong enough to cause $\langle \mu_1^z \rangle$ to point in the $-z$ direction, $\theta = 109 \pm 12^\circ$.

For the complete spin glass at $x=0.450$, Eq. (4) gives $\cos \alpha$ less than -1 , due mostly to uncertainties in the determination of $\langle B_{\text{hf}}^{\text{tot}}(\text{Sn}) \rangle$ and $\langle \mu_1^{\text{tot}} \rangle$ discussed previously. However, we know from the two cases of moderate frustration discussed above, that the Fe and Mn moments are aligned almost completely AF, therefore it seems reasonable to expect this behavior to continue into the spin-glass regime, so that $\langle \mu_1^{\text{tot}} \rangle$ is oriented completely AF with respect to $\langle \mu_{\text{Fe}}^{\text{tot}} \rangle$. We will take $\cos \alpha$ to be -1 in calculations of the total Mn moment at $x=0.450$.

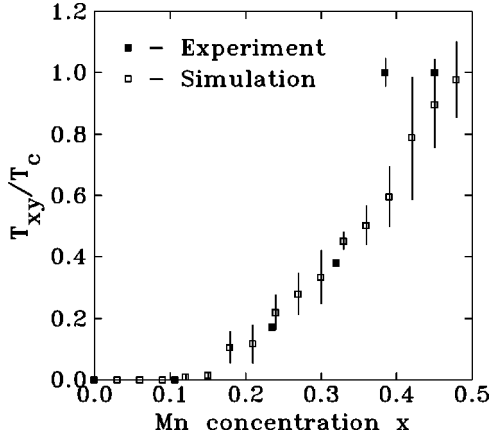


FIG. 9. Normalized comparison of magnetic phase diagram for $a\text{-(Fe}_{1-x}\text{Mn}_x\text{)}_{78}\text{Sn}_2\text{Si}_6\text{B}_{14}$ (solid symbols) with that derived from Monte Carlo simulations on a simple cubic site disordered Heisenberg model with nearest-neighbor interactions (open symbols) (Ref. 5). Note the excellent agreement with the main predictions of the simulations. Note also that at $x=0.385$ $a\text{-(Fe}_{1-x}\text{Mn}_x\text{)}_{78}\text{Sn}_2\text{Si}_6\text{B}_{14}$ has already reached a spin-glass state. This discrepancy is probably caused by inequality of absolute values of coupling constants J_{FeFe} , J_{MnMn} , and J_{FeMn} , which were assumed to be $+1$, -1 , and -1 , respectively, in the numerical work.

The most important conclusion of the present analysis is that in partially frustrated alloys the transverse components of the Mn moments $\langle\mu_{\text{Mn}}^{xy}\rangle$ order AF with respect to the transverse components of the Fe moments $\langle\mu_{\text{Fe}}^{xy}\rangle$. This same result was obtained in recent Monte Carlo simulations on a 3D Heisenberg model with nearest-neighbor interactions on a simple cubic lattice,⁵ in which site disorder was introduced by randomly replacing a fraction f of FM sites by AF sites. It was shown that in this case frustration can occur only when f is high enough to produce AF-AF nearest pairs which on average start to appear when $f=1/\text{NN}$. Increased frustration led to an increase in both the noncollinearity, and T_{xy} , and a decrease in T_c . While the longitudinal components of the spins within each sublattice were ordered FM on average, the frozen transverse components exhibited short-range AF correlations. Comparison of the normalized transverse spin freezing temperatures (T_{xy}/T_c) in Fig. 9 shows that our experimental data are in good agreement with the magnetic phase diagram of the site-disordered model.⁵ The exception is the point at $x=0.385$ which suggests that the system reaches the spin-glass regime earlier than the numerical model. In view of the excellent agreement over the rest of the phase diagram, the most likely explanation for the discrepancy lies with the details of the exchange distribution.

The numerical model assumed a simple $\pm J$ exchange distribution, however, this is unlikely to be the case in a real system. Indeed, the steep decline of T_c with x apparent in Fig. 4 suggests that the AF Mn-Mn interactions are significantly stronger than the FM Fe-Fe interactions. Fitting the concentration dependence of T_c assuming a simple mixing model^{11,53} and temperature-independent exchange constants, gives the following values: $J_{\text{FeFe}}=679\pm 9$ K, $J_{\text{MnFe}}=-227\pm 51$ K, and $J_{\text{MnMn}}=-1175\pm 84$ K, or approximately: $|J_{\text{MnMn}}|=5.2|J_{\text{MnFe}}|=1.7|J_{\text{FeFe}}|$, which is in agreement with the ratio obtained for crystalline $\gamma\text{-FeMn}$: $|J_{\text{MnMn}}|=6|J_{\text{MnFe}}|=2|J_{\text{FeFe}}|$ from measurements of magnetic

specific heat.⁵⁴ This large variation in exchange strengths has a number of consequences. The existence of distinct Mn and Fe sublattices assumed in our analysis and the overall AF Fe-Mn orientations derived from our analysis both require $|J_{\text{MnMn}}|$ and $|J_{\text{FeFe}}|$ to be larger than $|J_{\text{MnFe}}|$. The greater size of J_{MnMn} also leads to the frustration-independent canting angle of the average Mn moment (φ_{Mn} remains at $\sim 33^\circ$ with x rising from 0.235 to 0.320), while the weaker J_{FeFe} leads to a rapid increase in the canting angle of the Fe moments (φ_{Fe} increases from 29° to 45°). Finally, the greater magnitude of J_{MnMn} means that misaligned Mn moments will have a greater effect on the surrounding moments and so explains why long-range order is lost at lower doping levels in the experimental system than in the numerical model where $\pm J$ was used (see Fig. 9).⁵⁵

APPLICATION OF THE MODEL TO OTHER AMORPHOUS ALLOYS

It is interesting to apply the two-component model for hyperfine fields on ^{57}Fe and ^{119}Sn used in the present work to other iron-rich Fe glasses. The simplest will be to use it for alloys containing only one magnetic species, (e.g., Fe) where data on both $\langle B_{\text{hf}}(\text{Fe})\rangle$ and $\langle B_{\text{hf}}(\text{Sn})\rangle$ have been obtained on several partially and fully frustrated alloys. Estimates of the ratio $\mathcal{R}(T)$ for the cases of collinear alignment of transverse components can be made from formulas obtained after trivial mathematical transformations of the equations for $\langle B_{\text{hf}}^{\text{tot}}(\text{Fe})\rangle$ and $\langle B_{\text{hf}}^{\text{tot}}(\text{Sn})\rangle$ [Eqs. (4) and (5), respectively] and by introducing the xy component of the Fe moment as a fraction q of the total moment assuming that $\langle\mu_{\text{Fe}}^{\text{tot}}\rangle=\langle\mu_1^{\text{tot}}\rangle=\sigma$ in the case of FM alignment:

$$\mathcal{R}_{\text{FM}}(T)=(D-C)/(A+B), \quad (11)$$

and $\langle\mu_{\text{Fe}}^z\rangle=\langle\mu_1^z\rangle=\sigma$ in the case of AF alignment:

$$\mathcal{R}_{\text{AF}}(T)=[(D-C)\sqrt{1-q^2}]/\sqrt{A^2+(B^2+2AB)(1-q^2)}. \quad (12)$$

We note that $\mathcal{R}_{\text{FM}}(T)$ depends only on the field transfer coefficients, and not on any alloy parameters, while $\mathcal{R}_{\text{AF}}(T)$ also depends on q , i.e., larger tilting reduces the influence of the surrounding moments due to cancellation among the transverse components and \mathcal{R}_{AF} falls. For the case of spin-glass alignment of transverse components, we assume that $\langle\mu_{\text{Fe}}^z\rangle=\langle\mu_1^z\rangle=\sigma$. $\langle B_{\text{hf}}^{\text{tot}}(\text{Fe})\rangle$ and $\langle B_{\text{hf}}^{\text{tot}}(\text{Sn})\rangle$ can be obtained by statistical averaging of the xy components of the corresponding moments. We find that $\mathcal{R}_{\text{SG}}(T)$ also includes a dependence on $\langle\mu_{\text{Fe}}^{\text{tot}}\rangle$.

A study of $a\text{-Fe}_{92}\text{Zr}_7\text{Sn}$ showed a temperature independent \mathcal{R} , with no apparent anomaly at T_{xy} .²⁶ This was interpreted as indicating locally FM alignment of the transverse spin components. In order to apply our model to this data, we need values for the field transfer coefficients A – D . A sets the local contribution to $\langle B_{\text{hf}}(\text{Fe})\rangle$ from the Fe atom itself, and D gives the contribution to $\langle B_{\text{hf}}(\text{Sn})\rangle$ from domain magnetization. Both have been found to be independent of the alloy system used, so we have taken the values from the $a\text{-FeMn}$ alloys studied here, i.e., $A=-5.5$ T/ μ_B , $D=20$ T/ μ_B . B was then estimated as -9.5 T/ μ_B by applying Eq. (1) to the collinear $a\text{-Fe}_{89}\text{Zr}_{11}$ at 5 K where $\langle B_{\text{hf}}(\text{Fe})\rangle=23.4\pm 0.2$ T

and $\mu_{\text{Fe}} = \langle \mu_1 \rangle = 1.56 \pm 0.04 \mu_B$.³ Local AF or SG alignment of xy components with $q = 0.40$ [found for $a\text{-Fe}_{92}\text{Zr}_7\text{Sn}$ at 5 K (Ref. 26)] would result in $\langle B_{\text{hf}}^{\text{tot}}(\text{Fe}) \rangle = 22.0 \pm 0.5$ T which is somewhat less than the experimental value of 23.7 ± 0.2 T,³ and hence both correlation forms would appear to be unlikely. Assuming local FM alignment of the xy components and taking $\mathcal{R}_{\text{FM}} = 0.227$ [the average of experimental data obtained for $a\text{-Fe}_{92}\text{Zr}_7\text{Sn}$ in the temperature range from 5 K to 90 K (Ref. 26)], yields $C = 23.4$ T/ μ_B [from Eq. (11)]. The two-component model combined with the assumption of local FM alignment of xy components then predicts the experimentally observed²⁶ temperature-independent \mathcal{R} . By contrast, local AF alignment of xy components leads to a $\sim 2\%$ drop of $\mathcal{R}_{\text{AF}}(T)$ below T_{xy} , while local SG alignment leads to a $\sim 24\%$ increase in $\mathcal{R}_{\text{SG}}(T)$. Thus, combining the measured fields with the observed dependence of $\mathcal{R}(T)$ we find that the experimental data on the bond-frustrated $a\text{-Fe}_{100-x}\text{Zr}_x$ alloys are consistent only with local FM alignment of the transverse-spin components.

Substitution of Fe by Ni in $a\text{-Fe}_{90-x}\text{Ni}_x\text{Zr}_9\text{Sn}$ leads to a 10% increase in $\langle B_{\text{hf}}^{\text{tot}}(\text{Fe}) \rangle$ measured at 12 K on going from $x = 0$ to $x = 3$. This change is due to increased collinearity (reflected by a narrowing of the hyperfine field distribution and increased T_c) and an increase in the Fe moment (reflected by increased magnetization).³⁰ On going from $x = 1$ to $x = 3$, $\mathcal{R}(T)$ decreases from ~ 0.235 to ~ 0.223 while $\langle B_{\text{hf}}^{\text{tot}}(\text{Sn}) \rangle$ does not change. This behavior cannot be appropriately accounted for in the one component model which would predict an increase in $\langle B_{\text{hf}}^{\text{tot}}(\text{Sn}) \rangle$ caused by increases in collinearity and Fe moment. The two-component model however, predicts a greatly reduced effect. For locally FM correlations, μ_1^{tot} and σ will scale together as the Fe moment increases, and Eq. (2) shows that $\langle B_{\text{hf}}(\text{Sn}) \rangle$ is then proportional to $(D - C)\sigma$. The coefficients are close in size, greatly reducing the effects of an Fe moment increase. Equation (11) further shows that changes in collinearity do not affect \mathcal{R} . The net effect of the Fe moment increase on adding Ni is, therefore, a larger $\langle B_{\text{hf}}(\text{Fe}) \rangle$ at constant $\langle B_{\text{hf}}(\text{Sn}) \rangle$ and so \mathcal{R} decreases.

Finally, we consider the case of fully frustrated $a\text{-Fe}_{90}\text{Sc}_9\text{Sn}_1$ which exhibits a single transition to an isotropic spin-glass state.²⁷ $a\text{-FeSc}$ and $a\text{-FeZr}$ have many similarities including comparable compositions, and atomic radii (1.60 Å for Zr and 1.62 Å for Sc and Sn). The low temperature value of $\langle B_{\text{hf}}^{\text{tot}}(\text{Fe}) \rangle$ for $a\text{-Fe}_{90}\text{Sc}_{10}$ (and $a\text{-Fe}_{90}\text{Sc}_9\text{Sn}_1$) is 22.9 T,^{56,29} very close to the essentially composition-, and hence frustration-, independent 23.4 T found in $a\text{-Fe}_{100-x}\text{Zr}_x$.^{3,56} The observation that $\langle B_{\text{hf}}^{\text{tot}}(\text{Fe}) \rangle$ remains constant in $a\text{-Fe}_{100-x}\text{Zr}_x$ despite a 30% reduction in σ^3 is only consistent with locally FM correlated transverse components. Any other form would lead to some cancellation and a drop in $\langle B_{\text{hf}}^{\text{tot}}(\text{Fe}) \rangle$. In view of the many similarities between the $a\text{-FeSc}$ and $a\text{-FeZr}$ systems, it seems reasonable to expect that the correlations will continue to be FM as we cross into the spin glass. These expectations can be examined in more detail using the two-component hyperfine field model for $a\text{-Fe}_{90}\text{Sc}_9\text{Sn}_1$. $\langle \mu_1^{\text{tot}} \rangle = 0.22 \pm 0.02 \mu_B$ may be directly obtained from Eq. (5) (the second term is zero, as the average magnetization σ is zero, and $\langle B_{\text{hf}}^{\text{tot}}(\text{Sn}) \rangle = 5.1 \pm 0.2$ T was measured for $a\text{-Fe}_{90}\text{Sc}_9\text{Sn}_1$ at 12 K). This re-

sult is about half the value of $\langle \mu_1^{\text{tot}} \rangle = 0.41 \pm 0.05 \mu_B$ obtained by isotropic statistical averaging of 12 vectors $\langle \mu_{\text{Fe}}^{\text{tot}} \rangle = 1.55 \pm 0.05 \mu_B$ [using the moment obtained for the collinear $a\text{-Fe}_{89}\text{Zr}_{11}$ (Ref. 3)]. This assumption of random orientation also leads to a simulated value for $\langle B_{\text{hf}}^{\text{tot}}(\text{Fe}) \rangle = 9.1 \pm 0.5$ T (isotropic statistical average of the vector $A\langle \mu_{\text{Fe}}^{\text{tot}} \rangle$ and resulting isotropic statistical average of 12 vectors $B\langle \mu_{\text{Fe}}^{\text{tot}} \rangle$) which is again less than half of the value measured experimentally. Therefore, we can conclude that the absence of a bulk magnetization σ , does not translate into a fully random orientation of the moment vectors over the 1st NN shell.

CONCLUSIONS

The magnetic properties of site-frustrated $a\text{-(Fe}_{1-x}\text{Mn}_x)_{78}\text{Sn}_2\text{Si}_6\text{B}_{14}$ have been studied as functions of temperature and Mn concentration, x . Specifically, the detailed nature of the short-range correlations that develop below T_{xy} have been investigated using magnetic and nonmagnetic Mössbauer probes. At low x , the Mn moments couple AF with respect to the majority Fe moments and the alloy retains its collinear structure. Once x is large enough for Mn-Mn pairs to occur, exchange frustration develops and the magnetic order at $T = 0$ becomes noncollinear. On warming, the transverse components that lead to the noncollinearity melt at a well-defined temperature T_{xy} and the order is then collinear until it is lost on reaching T_c . The transverse components in this site-frustrated system were shown to exhibit AF correlations below T_{xy} , in strong contrast to the xy spin-glass order predicted for bond-frustrated materials. Furthermore, both the longitudinal z , and transverse xy components of the Fe moments are oriented antiparallel to their Mn counterparts. Indeed, this antiparallel tendency is so strong that it persists even in the fully frustrated $x = 0.450$ alloy. The general magnetic behavior as well as the AF character of the short-range correlations in the xy components are fully consistent with the results of Monte Carlo simulations on a three-dimensional site-disordered Heisenberg model with nearest-neighbor interactions.

We have shown that it is essential to use a two-component model in order to obtain a consistent description of the hyperfine fields at both magnetic and nonmagnetic Mössbauer probes. Such a model considers the effects of both the local Fe moment and the average moment on the 1st NN shell on the hyperfine field at magnetic ⁵⁷Fe sites, and the effects of both 1st NN and more distant shells on the hyperfine field at nonmagnetic ¹¹⁹Sn sites. The coefficients A , B , C , and D used here, were derived from a variety of experimental systems as consistent theoretical values are not available. Development of this model has allowed us to complete a rigorous analysis of the transferred hyperfine fields in $a\text{-(Fe}_{1-x}\text{Mn}_x)_{78}\text{Sn}_2\text{Si}_6\text{B}_{14}$ and so determine the nature of the local correlations among transverse components below T_{xy} . The conclusions of this analysis are robust, and while substantial changes in the field-transfer coefficients in Eqs. (1) and (2) degrade the fit quality and lead to variation in the Fe and Mn moments, they do not change the final result—antiparallel orientation of the Fe and Mn moments.

We have also applied the two-component model to a

range of bond-frustrated alloys, and shown that in this case, the transverse correlations below T_{xy} are strongly ferromagnetic in nature, at least on a first-neighbor length scale. In combination with bulk magnetization data, we can easily distinguish between FM, AF, or SG short-range transverse correlations on a local scale.

ACKNOWLEDGMENTS

This work was supported by grants from the Natural Sciences and Engineering Research Council of Canada and Fonds pour la formation de chercheurs et l'aide à la recherche, Québec.

- *Present Address: WIARDA, 7520 Wickam Rd., Knoxville, TN 37931.
- ¹M. Gabay and G. Toulouse, Phys. Rev. Lett. **47**, 201 (1981).
 - ²D.H. Ryan, Zin Tun, and J.M. Cadogan, J. Magn. Magn. Mater. **177-181**, 57 (1998).
 - ³H. Ren and D.H. Ryan, Phys. Rev. B **51**, 15 885 (1995).
 - ⁴J.R. Thomson, Hong Guo, D.H. Ryan, M.J. Zuckermann, and M. Grant, Phys. Rev. B **45**, 3129 (1992).
 - ⁵M. Nielsen, D.H. Ryan, Hong Guo, and M. Zuckermann, Phys. Rev. B **53**, 343 (1996).
 - ⁶C.L. Chien, J.H. Hsu, P.J. Viccaro, B.D. Dunlap, G.K. Shenoy, and H.S. Chen, J. Appl. Phys. **52**, 1750 (1981).
 - ⁷H. Keller, K.V. Rao, P.G. Debrunner, and H.S. Chen, J. Appl. Phys. **52**, 1753 (1981).
 - ⁸I. Merebeau, G. Jehanno, I.A. Campbell, F. Hippert, B. Hennion, and M. Hennion, J. Magn. Magn. Mater. **54-57**, 99 (1986).
 - ⁹J.A. Geohegan and S.M. Bhagat, J. Magn. Magn. Mater. **25**, 17 (1981).
 - ¹⁰G. Aepli, S.M. Shapiro, H. Maletta, R.J. Birgeneau, and H.S. Chen, J. Appl. Phys. **55**, 1628 (1984).
 - ¹¹K. Heinemann, C. Michaelsen, M. Fieber, and K. Bärner, J. Magn. Magn. Mater. **82**, 204 (1989).
 - ¹²T. Miyazaki, I. Okamoto, Y. Ando, and M. Takahashi, J. Phys. F **18**, 1601 (1988).
 - ¹³S. Yoon and J.G. Booth, J. Phys. F **7**, 1079 (1977).
 - ¹⁴T. Ersez, S.J. Kennedy, and T.J. Hicks, J. Phys.: Condens. Matter **7**, 8423 (1995).
 - ¹⁵D.C. Price, J. Phys. F **4**, 639 (1974).
 - ¹⁶S.G. Kang, H. Onodera, H. Yamamoto, and H. Watanabe, J. Phys. Soc. Jpn. **36**, 975 (1974).
 - ¹⁷Y. Nishihara, S. Ogawa, and S. Waki, J. Phys. Soc. Jpn. **42**, 845 (1977).
 - ¹⁸L.R. Walker, G.K. Wertheim, and V. Jaccarino, Phys. Rev. Lett. **6**, 98 (1961).
 - ¹⁹F. van der Woude and G.A. Sawatzky, Phys. Rep., Phys. Lett. **C12**, 335 (1974).
 - ²⁰A.E. Balabanov and N.N. Delyagin, Zh. Éksp. Teor. Fiz. **54**, 1402 (1968) [Sov. Phys. JETP **27**, 752 (1968)].
 - ²¹A.E. Balabanov and N.N. Delyagin, Zh. Éksp. Teor. Fiz. **57**, 1947 (1969) [Sov. Phys. JETP **30**, 1054 (1970)].
 - ²²N.N. Delyagin and E.N. Kornienko, Zh. Éksp. Teor. Fiz. **59**, 1524 (1970) [Sov. Phys. JETP **32**, 832 (1971)].
 - ²³N.N. Delyagin and E.N. Kornienko, Zh. Éksp. Teor. Fiz. **61**, 1946 (1971) [Sov. Phys. JETP **34**, 1036 (1972)].
 - ²⁴M.M. Abd-Elmeguid, H. Micklitz, R.A. Brand, and W. Keune, Phys. Rev. B **33**, 7833 (1986).
 - ²⁵A. Ait-Bahammou, C. Meyer, F. Hartmann-Boutron, Y. Gros, and I.A. Campbell, J. Phys. (Paris), Colloq. **49**, C8-1157 (1988).
 - ²⁶H. Ren and D.H. Ryan, Phys. Rev. B **47**, 7919 (1993).
 - ²⁷H. Ren and D.H. Ryan, J. Appl. Phys. **73**, 5494 (1993).
 - ²⁸D. Wiarda, H. Ren, and D.H. Ryan, Hyperfine Interact. **94**, 2303 (1994).
 - ²⁹D. Wiarda and D.H. Ryan, J. Appl. Phys. **76**, 6189 (1994).
 - ³⁰D. Wiarda and D.H. Ryan, J. Appl. Phys. **76**, 6377 (1994).
 - ³¹D.H. Ryan, in *Recent Progress in Random Magnets*, edited by D.H. Ryan (World Scientific, Singapore, 1992).
 - ³²K. Handrich, Phys. Status Solidi **32**, K55 (1969).
 - ³³D.H. Ryan, J.M. Cadogan, and S.J. Kennedy, J. Magn. Magn. Mater. **162**, 55 (1996).
 - ³⁴Brent Fultz, in *Mössbauer Spectroscopy Applied to Magnetism and Materials Science*, edited by Gary J. Long and Fernande Grandjean (Plenum, New York, 1993), Vol. 1.
 - ³⁵M.E. Elzain, D.E. Ellis, and D. Guenzburger, Phys. Rev. B **34**, 1430 (1986).
 - ³⁶H. Ebert, H. Winter, D.D. Johnson, and F.J. Pinski, J. Phys.: Condens. Matter **2**, 443 (1990).
 - ³⁷S. Blügel, H. Akai, R. Zeller, and P.H. Dederichs, Phys. Rev. B **35**, 3271 (1987).
 - ³⁸S. Mager, E. Weiser, T. Zemcik, O. Schneeweiss, P.N. Stetsenko and V.V. Surikov, Phys. Status Solidi A **52**, 249 (1979).
 - ³⁹M. Wolf, S. Mager, P.N. Stetsenko, V.V. Surikof, and S.I. Kasatkin, Zh. Éksp. Teor. Fiz. **71**, 1529 (1976) [Sov. Phys. JETP **44**, 800 (1976)].
 - ⁴⁰S.M. Dubiel and W. Zinn, Phys. Rev. B **26**, 1574 (1982).
 - ⁴¹D.A. Shirley and G.A. Westenbarger, Phys. Rev. **138**, A170 (1965).
 - ⁴²Y. Koi, A. Tsujimura, T. Hihara, and T. Kushida, Proceedings of the International Conference on Magnetism and Crystallography, (Kyoto, 1961) [J. Phys. Soc. Jpn. **17**, Suppl. BI, 96 (1962)].
 - ⁴³Le Dang Khoi, P. Veillet, and I.A. Campbell, J. Phys. F **5**, 2184 (1975).
 - ⁴⁴C.C.M. Campbell, T. Birchall, and J.C. Suits, J. Phys. F **7**, 727 (1977).
 - ⁴⁵N.N. Delyagin, V.I. Krylov, and V.I. Nesterov, Zh. Éksp. Teor. Fiz. **79**, 1049 (1980) [Sov. Phys. JETP **52**, 532 (1980)].
 - ⁴⁶N.N. Delyagin, Yu.D. Zonnenberg, V.I. Krylov, and V.I. Nesterov, Hyperfine Interact. **11**, 65 (1981).
 - ⁴⁷M. Akai, H. Akai, and J. Kanamori, J. Phys. Soc. Jpn. **54**, 4246 (1985).
 - ⁴⁸We explicitly include the $-$ sign in this equation to emphasize the opposite signs of the two contributions to the ^{119}Sn hyperfine field. This choice makes both C and D in Eq. (2) positive. We recognize that the hyperfine field at both the ^{57}Fe and ^{119}Sn sites is in fact negative, but omit the many $-$ signs for clarity.
 - ⁴⁹Y. Waseda and H.S. Chen, Phys. Status Solidi A **49**, 387 (1978).
 - ⁵⁰Y. Endoh and Y. Ishikawa, J. Phys. Soc. Jpn. **30**, 1614 (1971).
 - ⁵¹P.H. Dederichs, R. Zeller, H. Akai, and H. Ebert, J. Magn. Magn. Mater. **100**, 241 (1991).
 - ⁵²A.K. Sinha, J. Appl. Phys. **42**, 338 (1971).
 - ⁵³I.V. Medvedeva, Yu.S. Bersenev, A.A. Ganin, K. Baerner, J.-W. Schuenemann, and K. Heinemann, J. Magn. Magn. Mater. **124**, 293 (1993).
 - ⁵⁴T. Hashimoto and Y. Ishikawa, J. Phys. Soc. Jpn. **23**, 213 (1967).
 - ⁵⁵The onset of T_{xy} depends only on the presence of Mn-Mn pairs and so is unaffected by relative exchange strengths.
 - ⁵⁶D.H. Ryan, J.O. Strom-Olsen, W.B. Muir, J.M. Cadogan, and J.M.D. Coey, Phys. Rev. B **40**, 11 208 (1989).